Withdrawal and dip coating of an object from a yield-stress reservoir

Wilbert J. Smit,[1,2] Christophe Kusina,[1,3] Annie Colin,[1,4,*] and Jean-François Joanny[5,6]
[1]*Chimie Biologie et Innovation, ESPCI Paris, Université PSL, CNRS, 75005 Paris, France*
[2]*Univ Lyon, Ens de Lyon, Univ Claude Bernard, CNRS, Laboratoire de Physique, 69342 Lyon, France*
[3]*L'Oréal, 188 rue Paul Hochart, 94550 Chevilly-Larue, France*
[4]*Centre de Recherche Paul Pascal, CNRS, Université de Bordeaux, 115 Avenue Schweitzer, 33600 Pessac, France*
[5]*Physico Chimie Curie, Institut Curie, PSL University, 26 rue d'Ulm, 75005 Paris, France*
[6]*Collège de France, 11 place Marcelin Berthelot, 75005 Paris, France*

(Received 8 November 2020; accepted 2 June 2021; published 14 June 2021)

The dip-coating process consists of withdrawing immersed objects from a liquid reservoir. After withdrawal, a significant layer of liquid remains on the object. Various industrial processes (food and beverage industry, automotive industry) use this technique to coat or treat surfaces. Recent studies have shown that the thickness of deposit is determined by the flow inside the reservoir for yield-stress fluids. This is different from the behavior of simple liquids for which the coating thickness is solely determined by the flow inside the meniscus. In this work, we reexamine this question and propose a complete phase diagram linking the Newtonian case and the yield-stress fluid case. We provide asymptotic scaling laws for extreme cases. A good agreement with experiments is obtained.

DOI: 10.1103/PhysRevFluids.6.063302

I. INTRODUCTION

In everyday life, various types of yield-stress fluids are employed as adhesives, paints, gels, pastes, and creams. They respond elastically to small applied stresses and flow as viscous fluids if the applied stress exceeds the critical yield stress. In many applications, yield-stress fluids are spread on a solid substrate. At home, examples are putting chocolate spread on a toast or coating of eyelashes by mascara. A controlled spreading technique is dip coating in which a film is deposited by withdrawing an immersed object from a fluid reservoir as sketched in Fig. 1. The method is low-cost, waste-free, and easy to scale up [1]. It is broadly used in a wide variety of industrial applications that range from manufacturing to the food industry [2]. In academic research, the dip-coating technique is frequently employed to prepare thin films from sol-gel precursors [3–5]. It is of major interest to master the thickness of the coating film, which generally depends on several physical parameters: fluid properties, withdrawal velocity and shape of the withdrawn object. The flow extends from the reservoir to the deposited film through a connecting area called the meniscus. The shape of the meniscus is given by the balance between gravity and surface tension for simple liquid or gravity, surface tension and yield stress for yield-stress fluids. A static meniscus is connected to the film of constant thickness by a zone of variable thickness coined as the dynamic meniscus. It is usually admitted that the shape of the part of the meniscus in contact with the reservoir is not modified by the liquid flow. The deposit thickness is controlled by the a balance between viscous and capillary forces in the dynamic meniscus [6–9]. This description has been validated experimentally on many Newtonian fluids [8,9]. For yield-stress fluids with a large yield

*annie.colin@espci.fr

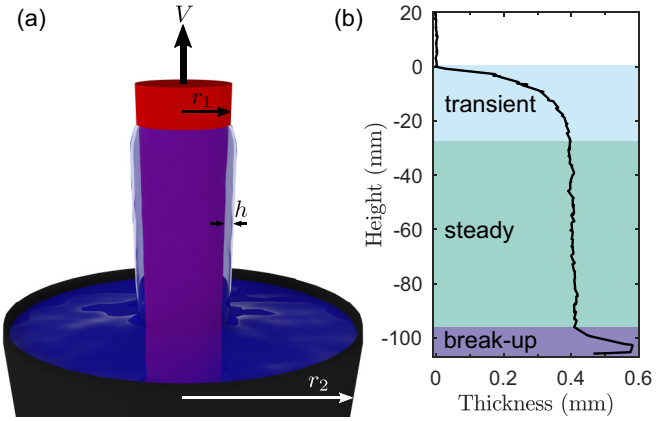

FIG. 1. (a) Schematic of the dip-coating experiment: a rod of radius r_1 is pulled out with velocity V from a cylindrical liquid reservoir of radius r_2, which deposits a coating film of thickness h. (b) Typical thickness profile resulting from the dip coating. The coating profile can be divided into regions in a transient regime, a steady regime, and break-up regime (see text).

stress, previous studies have revealed that the flow inside the reservoir plays a role [10–12]. In other words, for high yield stress values, the amount of liquid pulled out of the reservoir is not large enough to feed the film as would be required by the static meniscus. In this situation, the thickness of the coating is determined by the flow inside the reservoir and not by the flow inside the meniscus [13]. There are currently no descriptions that unify these limiting behaviors. Theoretical approaches have considered only the situations where the process is determined by the flow either in the bath [12,13] or in the meniscus [6–9]. Furthermore, no simple criterion on the yield-stress exists that distinguishes whether the thickness of the deposited film depends on the flow in the bath and/or the flow in the meniscus The originality of our work is to provide such a criterion and to propose a description that bridges the gap between the two limiting behaviors.

In this work we study a cylindrical geometry sketched in Fig 1 of a rod of radius r_1 pulled out of a cylindrical bath of yield stress fluid of radius r_2. The limiting case where the object is a plate ($r_1 \to \infty$) is treated in the Supplemental Material (SM) [14]. The choice of a cylindrical geometry comes from the fact that the bath plays an important role in the size of the deposit. Indeed, the flow is more complex in a square or rectangular bath. This argument justifies the theoretical positioning. Experimentally, the circular geometry is not necessarily the most used. Another advantage is that the centering allows to obtain a homogeneous deposit. The position of the object and their centering in the bath are crucial and can induce inhomogeneous deposits. In terms of applications, a very large bath if not circular is favorable.

The current work is structured as follows: in Sec. II we introduce the hydrodynamic equations and explain our strategy to bridge the gap between the two limiting behaviors. Section III considers the situation where the flow in the reservoir is the mechanism that governs the process, and Sec. IV considers the situation where the flow in the meniscus dominates. In both situations, we provide solutions for the thickness of the deposit in the asymptotic limits, i.e., for both low or large values of the yield stress. Then we present a comprehensive diagram drawing the boundaries between these two regimes in Sec. V. Section VI is devoted to a comparison with experiments. The final section displays the conclusions and the outlook of this work.

II. FROM RESERVOIR ONTO COATING

When an object is withdrawn from a fluid reservoir, a fluid flow is created. In this work, we assume that flow is steady, i.e., that the velocity and the stress do not depend on time. An analysis

of the conditions to reach this steady state is given in Appendix A. We assume that the inertial stresses are negligible compared to the deviatoric stress tensor components, i.e., low Reynolds number Re. This corresponds to a situation where $\mathrm{Re} = \frac{\rho V^2}{\tau_c} \ll 1$ with ρ the density of the fluid, V the withdrawal velocity, and τ_c the yield stress. Under these hypotheses, the momentum balance equation writes

$$\boldsymbol{\nabla} \cdot \boldsymbol{\tau} - \boldsymbol{\nabla} P + \rho \mathbf{g} = 0, \tag{1}$$

with P the fluid pressure, ρ the fluid density, and g the gravitational acceleration. The deviatoric stress tensor $\boldsymbol{\tau}$ depends on the rheological properties of the fluid. The modeling of yield-stress fluids is still a subject of debate. Various viscoplastic models have been proposed and we refer to Fraggedakis *et al.* [15] for a recent review. The Herschel-Bulkley model successfully describes experimental observations of steady flows of liquid foams, emulsions, and microgels [16–19]. A detailed analysis of the conditions for its validity is given in Appendix A. The constitutive equation of this model reads

$$\dot{\gamma} = \max\left(0, \frac{|\boldsymbol{\tau}| - \tau_c}{k}\right)^{\frac{1}{n}} \frac{\boldsymbol{\tau}}{|\boldsymbol{\tau}|}, \tag{2}$$

where $\dot{\gamma}$ is the shear rate, k is the consistency parameter, and $n > 0$ is the power index. The shear-thinning behavior is associated to $0 < n < 1$. This model reduces to the Bingham model when $n = 1$. Shear-thickening behavior corresponds to $n > 1$ but is more unusual [20].

This set of equations has to the completed by boundary conditions. We assume in this paper that the solid-liquid interface is impermeable and consider the case of an object vertically withdrawn from a fluid reservoir with velocity V. At the object-fluid interface, the fluid velocity is $\mathbf{v} = V\hat{\mathbf{z}}$ and at the reservoir-fluid boundary $\mathbf{v} = 0$. At the free surface of the film, the tangential stress vanishes and the value of the normal stress is given by Laplace's law:

$$P - P_0 - \Gamma\mathcal{H} = \hat{\mathbf{n}} \cdot \boldsymbol{\tau}\hat{\mathbf{n}} = 0, \tag{3}$$

where P is the pressure inside the meniscus, P_0 is the atmospheric pressure, Γ is the fluid/air surface tension, $\mathcal{H}$ is the curvature of the interface, and $\hat{\mathbf{n}}$ is the normal unit vector to the interface.

Beyond the different parameters that define the flow, the problem is made complex by the geometry. Part of the flow takes place in the bath, and part of the flow takes place in the film. In classical descriptions for simple fluids, the flow in the bath is not taken into account. The hypothesis is made of the existence of a static meniscus that feeds the film, which is not perturbed by the flow. The static meniscus is however sufficient to drain enough material and feed the film. This description is no longer valid for yield-stress fluids for which a large portion of the sample is jammed. The value of the stress borne by the sample is in many locations smaller than the yield stress value. This is in particular the case for the part of the sample in contact with air or in the center of the bath. The amount of material coating the rod is therefore limited by the amount of material that can flow from the bath. Surface tension and meniscus play a minor role in this situation. In the following we will proceed with this hypothesis. We study separately the two limiting situations: the situation where the flow is driven by the properties of the bath and the situation where the flow is driven by the meniscus. To predict the thickness of the deposit in the first situation, we analyze the thickness of the deposit on a rod from a yield-stress fluid subjected to viscous driving forces and gravity. We set as a boundary condition at the bottom of the rod the amount of liquid per unit time delivered by the bath. To eliminate the role of the meniscus, we assume that the surface tension vanishes. The second situation is analyzed assuming the existence of a static meniscus with a shape set by a balance between surface tension, yield stress, and gravity. In this situation we analyze the flow in the dynamic meniscus and determine the pressure drop using the static shape of the meniscus. We then select the limiting process by comparing the obtained thickness. The situation giving the thinner deposit is the limiting process. This method allows us to obtain a general diagram for the various possible values of the thickness of the deposit as a function of both the geometrical parameters of

the experiments and the rheological parameters of the yield stress fluid. As we show below, the study of these limiting situations remains complex. To advance we propose in each of the two cases to make a dimensional analysis based on the Buckingham π theorem, which indicates the minimal number of dimensionless parameters that describe the phenomenon. We then determine regions where the coating process involves a dominant physical phenomenon. In each region, we estimate the thickness of the deposit. Depending on the case, these regions are defined by the fact that the chosen dimensionless parameters are larger than one or smaller than one or by the fact that some combination of these parameters is larger or smaller than one. These criteria are used to find the equation of the boundaries between the regions.

III. COATING DRIVEN BY THE FLOW IN THE RESERVOIR

In this section, we consider the case where the thickness of the coating film on a cylinder of radius r_1 pulled at a velocity V from a reservoir of yield stress fluid of radius r_2, is driven by the flow in the reservoir. In this situation the meniscus plays no role. The characteristic parameters involved in the flow are h the thickness of the deposit, r_1 the radius of the rod, r_2 the radius of the reservoir, ρg the gravity force by unit volume, V the rod velocity, and the yield stress τ_c. These six parameters involve three fundamental units. According to Buckingham's π theorem, a set of three dimensionless parameters are required to describe the flow: we choose here the confinement parameter $\mathrm{Co} = (r_2 - r_1)/r_1$, the Bingham number $\mathrm{Bm} = \frac{\tau_c}{k}(\frac{r_2-r_1}{V})^n$ (the ratio of the yield stress by the viscous stress), and $\bar{\mathrm{Y}} = \tau_c/(r_1\rho g)$ (the ratio of the yield stress to the gravitational stress). In order to find the dependence of the coating thickness on the dimensionless parameters $\{\mathrm{Co}, \mathrm{Bm}, \bar{\mathrm{Y}}\}$, we proceed through different steps. First, we link Co to the amount of liquid going out from the reservoir. We evidence two situations, one occurring for $h > h^*$ and another for $h < h^*$, where h^* is the thickness of deposit at which the stress at the rod's surface equals yield stress $-\tau_c$. Then we calculate the amount of liquid going out of the reservoir as a function of Co and Bm. Finally, we predict the thickness of the deposit by regrouping these calculations.

A. Link between the thickness of the deposit and the amount of liquid that goes out from the reservoir as a function of time

The pressure gradient outside the bath in the flat part of the meniscus vanishes and the shear stress profile in the film is given by the force balance on a fluid annulus of height $\mathrm{d}z$ which has an internal radius $r \geqslant r_1$ and an external radius $r_1 + h$ at the free surface,

$$\tau_{rz}(r) = \frac{\rho g r}{2} - \frac{\rho g (r_1 + h)^2}{2r}. \tag{4}$$

Let us call h^* the thickness of the deposit at which the stress on the rod equals the yield stress $-\tau_c$:

$$\frac{h^*}{r_1} = -1 + \sqrt{1 + 2\frac{\tau_c}{r_1 \rho g}}. \tag{5}$$

If the collected deposit h is smaller than h^*, the film is jammed on the rod, and we are left with the mass conservation equation

$$\left[\frac{\pi (r_1 + h)^2}{2} - \frac{\pi r_1^2}{2}\right] V_{\mathrm{coating}} = Q_{\mathrm{bath}}. \tag{6}$$

The coating velocity V_{coating} is larger than the withdrawal velocity V of the rod, because the withdrawal leads to a lowering of the liquid level of the reservoir. V_{coating} is the fluid velocity in the reference frame of the fluid level of the reservoir. If $h < h^*$, V_{coating} is constant over the film's thickness and the velocity profile $v_{\mathrm{coating}}(r)$ does not depend on the radial position r. Note that $h < h^*$ corresponds to the situation where the system is jammed meaning that the absolute value of the shear stress nowhere exceeds the yield stress. If $h > h^*$, the mass conservation becomes tricky

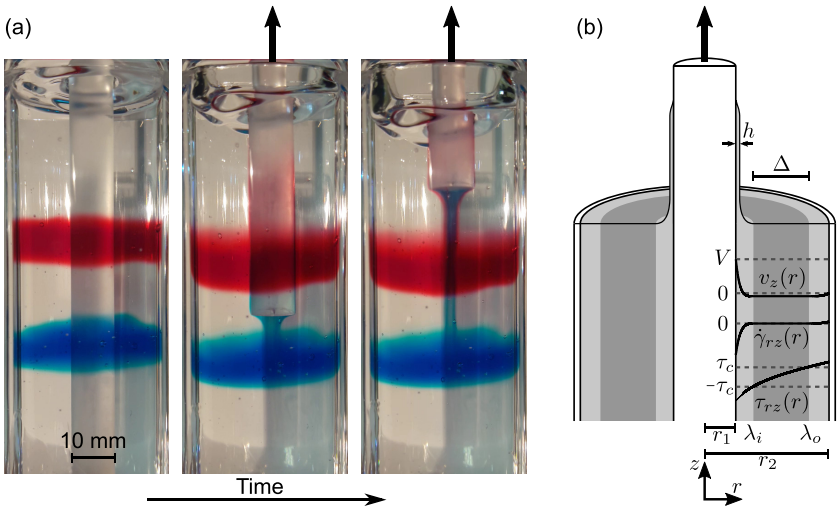

FIG. 2. (a) Sequential pictures of a dip-coating experiment with a Carbopol gel with $n = 0.35$ and $\mathrm{Bm} = 4$. Horizontal layers are colored by food coloring to indicate the fluid flow, which is vertical away from the meniscus and the end of the rod. (b) Schematic cross sections of a steady fluid flow with $n = 0.35$ and $\mathrm{Bm} = 1$ for a cylindrical geometry with $r_1 = r_2/4$. Inside the reservoir, the yielded regions are indicated light-shaded, and the unyielded regions are shown dark-shaded.

since part of the liquid going out from the reservoir drains back into the reservoir. We get

$$\int_{r_1}^{h+r_1} 2\pi r v_{\mathrm{coating}}(r)\, dr \leqslant Q_{\mathrm{bath}} \dot{\gamma}_{rz}(r) = \begin{cases} 0 & \text{for } r \geqslant h^* \\ -\frac{1}{k}\left[\tau_c + \frac{\rho g r}{2} - \frac{\rho g (r_1+h)^2}{2r}\right]^{\frac{1}{n}} & \text{for } r < h^* \end{cases}. \tag{7}$$

Solving these equations requires the calculation of the fluid flow inside the reservoir. For highly symmetric geometries, the flow inside the reservoir can be calculated semianalytically. Here we discuss the axisymmetric case of a cylinder vertically withdrawn from a concentric cylindrical reservoir. A similar analysis of the two-dimensional dip coating problem on a plate is provided in the SM [14]. It should be noted, however, that from the moment that the flow in the bath is important, having a nonsymmetrical or noncentered geometry has repercussions on the film. The thickness of the film is no longer homogeneous, and one side of it might be thicker than another. The analysis of this case goes beyond the scope of this work.

B. Flow through concentric annuli, calculation of the amount of fluid leaving the reservoir

The withdrawal of a rod from a concentric reservoir of yield-stress fluid gives rise to a vertical flow in the z direction in the fluid regions away from the meniscus and the end of the rod [Fig. 2(a)]. The only nonvanishing stress component is the shear stress τ_{rz}. At low Reynolds number Re, i.e., when the inertial stresses are negligible compared to the deviatoric stress tensor components, the inertial terms vanish. This corresponds to a situation where $\mathrm{Re} = \rho V^2/\tau_c \ll 1$ with V the withdrawal velocity. The resulting Stokes equation for the momentum balance reads

$$-\rho g - \frac{\partial P}{\partial z} + \frac{1}{r}\frac{\partial r \tau_{rz}}{\partial r} = 0, \tag{8}$$

with r the radial coordinate and z the vertical axis [the notation is detailed in Fig. 2(b)].

By integration, the general solution for a non-Newtonian fluid with a yield stress τ_c flowing through a concentric annulus can be obtained [21]:

$$\tau_{rz} = \frac{\tau_c}{\Delta}\left(r - \frac{\lambda^2}{r}\right). \tag{9}$$

Here $\Delta = 2\tau_c/(\rho g + \partial P/\partial z)$ and λ is a so far undetermined integration constant, corresponding to the radius where the shear stress vanishes.

The positions of the yield surfaces (λ_i and λ_o) are given by the conditions $\tau_{rz}(\lambda_i) = -\tau_c$ and $\tau_{rz}(\lambda_o) = \tau_c$, respectively. The length $\Delta = \lambda_o - \lambda_i$ is then the width of the plug flow region, and the length $\lambda = \sqrt{\lambda_i \lambda_o}$ is the geometric mean of the yield radii. The shear stress field is hence given by

$$\tau_{rz} = \frac{\tau_c}{\lambda_o - \lambda_i}\left(r - \frac{\lambda_i \lambda_o}{r}\right). \tag{10}$$

The unknown positions of the yield surfaces λ_o and λ_i are determined from the boundary conditions of the velocity profile and mass conservation. The velocities at the two boundaries ($v_z(r_1) = V$ and $v_z(r_2) = 0$) yield the integration constants of the shear rate:

$$V + \int_{r_1}^{r_2} \dot{\gamma}\, dr = 0. \tag{11}$$

Because of mass conservation, the volume of the retracted rod is compensated by a downwards flux in the reservoir. This imposes that

$$-\pi r_1^2 V = 2\pi \int_{r_1}^{r_2} r v_z(r)\, dr = \pi [r^2 v_z(r)]_{r_1}^{r_2} - \pi \int_{r_1}^{r_2} r^2 \dot{\gamma}\, dr, \tag{12}$$

where the second equality is obtained by an integration by parts. Assuming no-slip velocity boundary conditions, this last equation can be rewritten as

$$\int_{r_1}^{r_2} r^2 \dot{\gamma}\, dr = 0. \tag{13}$$

Hence, we simultaneously need to solve Eqs. (11) and (13) for the unknowns λ_i and λ_o. The shear rate is calculated using the Herschel-Bulkley model:

$$\dot{\gamma}_{rz}(r) = \begin{cases} -\left[\frac{\tau_c}{k(\lambda_o - \lambda_i)}\right]^{\frac{1}{n}} \left(\frac{\lambda_i \lambda_o}{r} - r + \lambda_i - \lambda_o\right)^{\frac{1}{n}} < 0 & \text{for} \quad r_1 \leqslant r < \lambda_i \\ 0 & \text{for} \quad \lambda_i \leqslant r \leqslant \lambda_o \\ \left[\frac{\tau_c}{k(\lambda_o - \lambda_i)}\right]^{\frac{1}{n}} \left(r - \frac{\lambda_i \lambda_o}{r} + \lambda_i - \lambda_o\right)^{\frac{1}{n}} > 0 & \text{for} \quad \lambda_o < r \leqslant r_2 \end{cases}. \tag{14}$$

The determination of the yield surfaces is then reduced to finding the roots of the following functions of $\lambda_{i,o}$:

$$\mathcal{F}(\lambda_i, \lambda_o) = \left[\frac{k(\lambda_o - \lambda_i)}{\tau_c}\right]^{\frac{1}{n}} V - \int_{r_1}^{\lambda_i} f(r, \lambda_i, \lambda_o)\, dr + \int_{\lambda_o}^{r_2} f(r, \lambda_i, \lambda_o)\, dr, \tag{15}$$

$$\mathcal{G}(\lambda_i, \lambda_o) = \int_{r_1}^{\lambda_i} r^2 f(r, \lambda_i, \lambda_o)\, dr - \int_{\lambda_o}^{r_2} r^2 f(r, \lambda_i, \lambda_o)\, dr \tag{16}$$

with

$$f(r, \lambda_i, \lambda_o) = \left(\left| r - \frac{\lambda_i \lambda_o}{r} \right| + \lambda_i - \lambda_o\right)^{\frac{1}{n}}. \tag{17}$$

The function $\mathcal{F}$ follows from the boundary conditions on the velocity [Eq. (11)] and the function $\mathcal{G}$ follows from mass conservation [Eq. (13)].

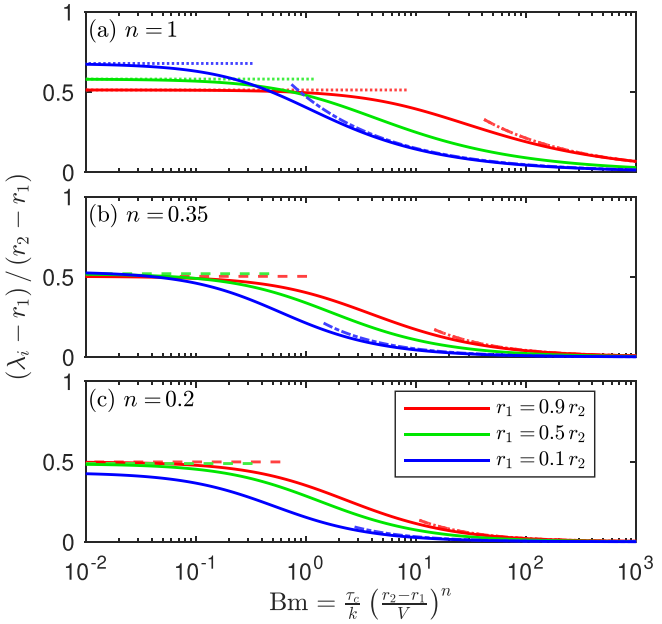

FIG. 3. Normalized width of the inner liquid zone in steady flow for different power index n and ratio r_1/r_2 as a function of Bingham number Bm. Dotted lines denote the low-Bm limit for $n = 1$ [Eq. (B2)]. Dashed lines denote the low-Bm approximation for a reservoir with a narrow gap [Eq. (B4)]. Blue dotted-dashed lines denote the high-Bm approximation for a large reservoir [Eq. (B14)]. Red dotted-dashed lines denote the high-Bm approximation for a reservoir with a small gap [Eq. (B10)].

In order to solve numerically this problem, we perform a double iteration along the lines of Fordham *et al.* [22]. The outer iteration provides a zero of $\mathcal{F}$, to iterate the value of λ_i that lies in the range $r_1 \leqslant \lambda_i < \lambda_*$ where λ_* is the limit to which both λ_i and λ_o converge when the Bingham number $\mathrm{Bm} = \frac{\tau_c}{k}(\frac{r_2 - r_1}{V})^n$ tends to zero. Its value is found by solving

$$\int_{r_1}^{\lambda_*} r^2 f(r, \lambda_*, \lambda_*)\, dr = \int_{\lambda_*}^{r_2} r^2 f(r, \lambda_*, \lambda_*)\, dr. \tag{18}$$

The outer iteration provides a solution of $\mathcal{G} = 0$ given an iterate λ_i, to iterate λ_o, which lies in the range $\lambda_i < \lambda_o \leqslant r_2$. Typical velocity and shear-stress profiles are plotted in Fig. 2. In our previous work, we showed a quantitative agreement of the model with experimental velocity profiles [13].

The flow inside the reservoir depends on three independent length scales [r_1, r_2, and the rheological length $V(k/\tau_c)^{1/n}$]. Hence, according to Buckingham's π theorem, a set of two dimensionless parameters is required to describe the flow: we choose r_1/r_2 and the Bingham number Bm. Note that the flow in the reservoir only depends on the ratio τ_c/k and not on k and τ_c individually. In Fig. 3 we show the width of the inner liquid zone ($\delta = \lambda_i - r_1$) normalized by the channel width ($r_2 - r_1$) as function of Bm. The normalized width of the inner liquid zone decreases with increasing Bm.

C. Steady state coating without drainage ($h < h^*$)

When the rod is withdrawn from the liquid reservoir, the fluid dragged along forms a coating layer. An upper bound of the coating thickness is obtained when all the fluid in the sheared layer between r_1 and λ_i deposits onto the rod. This occurs when the value of the yield stress is sufficiently high, i.e., when h is smaller than h^*.

The coating velocity V_{coating} is given by $V - v_z(\lambda_i)$. When all the fluid in the yielded layer is deposited on the rod leaving a layer of thickness h, mass conservation leads to

$$\pi\left[(r_1+h)^2 - r_1^2\right][V - v_z(\lambda_i)] = 2\pi \int_{r_1}^{\lambda_i} r[v_z(r) - v_z(\lambda_i)]\, dr. \tag{19}$$

The thickness of the coating is obtained by integration by parts of Eq. (19):

$$h = -r_1 + \sqrt{\frac{\int_{r_1}^{\lambda_i} r^2 \dot{\gamma}_{rz}(r)\, dr}{\int_{r_1}^{\lambda_i} \dot{\gamma}_{rz}(r)\, dr}}. \tag{20}$$

It is not possible to obtain an analytical relationship between the thickness of the fluidized layer and the coating thickness for all values of the index n for a Herschel-Bulkley fluid. In the special case of a Bingham fluid (Herschel-Bulkley model with $n = 1$), Eq. (20) gives

$$h_{n=1} = -r_1 + (\lambda_i - r_1)\sqrt{\frac{3r_1^2 + 2r_1(\lambda_i + 2\lambda_o) + \lambda_i(\lambda_i + 2\lambda_o)}{-6(\lambda_i - r_1)(2\lambda_o - \lambda_i + r_1) + 12\lambda_i\lambda_o \ln\frac{\lambda_i}{r_1}}}. \tag{21}$$

When λ_i/r_1 is close to unity, we make a series expansion of λ_i around r_1. By performing a change of variable $p = 1 - r/\lambda_i$ in both integrals of Eq. (20), we obtain up to first order:

$$h \simeq \frac{n}{1+2n}(\lambda_i - r_1). \tag{22}$$

Note that this expression is the same as that obtained for the coating of a plate given in Ref. [13]: when the width of the inner sheared layer $(\lambda_i - r_1)$ is small with respect to the rod radius r_1, curvature effects can be neglected.

In general, the coating thickness h depends nonlinearly on the length scales r_1, r_2, and $V(k/\tau_c)^{1/n}$. However, in extreme cases of low and high values of the dimensionless ratio r_1/r_2 and the Bingham number Bm, asymptotic power laws for the width of the liquid zone and the coating thickness can be obtained. The derivations of the asymptotic formulas and their ranges of validity are given in Appendix B. Five regimes (I–V) are distinguished. When the fluid inside the gap is strongly sheared, the yield stress character can be neglected and asymptotic limits are obtained for high r_1/r_2 (I) and for low r_1/r_2 (II). The asymptotic limits in I and II only depend on r_1, r_2 and n. When the fluid inside the gap is weakly sheared, a major part of the fluid in the bath is unyielded and the coating thickness decreases with increasing Bm. Regimes III–V are valid for high, low, and extremely low r_1/r_2, respectively. In regimes IV and V the coating thickness is independent on the bath radius r_2.

To summarize, an overview of the asymptotic limits for $\frac{1}{3} \leqslant n < 1$ is given in Fig. 4. The domain boundaries are obtained by equating the asymptotic limits. For $n = 1$, an exact asymptotic solution for the low-Bm limits I–II can be obtained [Eqs. (B2) and (B3)].

D. Steady state coating subject to drainage ($h > h^*$)

In the limit where the coating is dominated by the flow in the reservoir, the film is in general unyielded if the absolute value of the yield stress exceeds the gravitational stress. However, if the gravitational field is strong enough, a fraction of the film close to the rod is draining, which tends to decrease the coating thickness. We would like that stress that drainage can already occur in the meniscus where the fluid has a thickness up to $\delta = \lambda_i - r_1$, i.e., significantly thicker than the final coating thickness h. This regime has already been studied for a plate geometry by Maillard *et al.* [12] Mass conservation and momentum balance allow us to write

$$\int_{r_1}^{h+r_1} 2\pi r V_{\text{coating}}(r) dr \leqslant Q_{\text{bath}}, \tag{23}$$

$$r_1 \tau_{rz}(r_1) = \frac{\rho g}{2}\left[r_1^2 - (r_1 + h_g)^2\right], \tag{24}$$

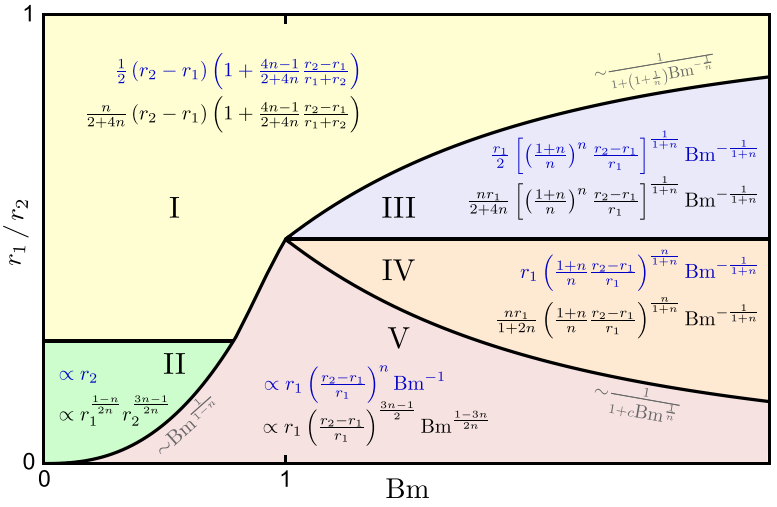

FIG. 4. Asymptotic limits of the width of the liquid zone $\delta = \lambda_i - r_1$ (blue) and the reservoir-flow coating thickness h (black) for $\frac{1}{3} < n < 1$. The parameter space can be divided up into domains I–V (see Appendix B). Solid lines indicate the typical shape of the domain boundaries, whose nontrivial dependencies are given in gray. c denotes a constant.

respectively, where h_g is the coating thickness affected by gravitation drainage. Solving these coupled equations is complex and out of the scope of the current work. We give here only an estimation of the parameters for which gravitational drainage becomes important.

To find the boundary between regime IV/V and the regime where gravity plays a role we use the following procedure. If the thickness h calculated from of Eq. (20) is larger than h^*, the thickness of deposit is governed by drainage due to gravity. We thus define a zone E (see Fig. 5) at low $\bar{\mathrm{Y}}$ where the thickness of deposit is governed by gravity after the withdrawal of the rod of the reservoir.

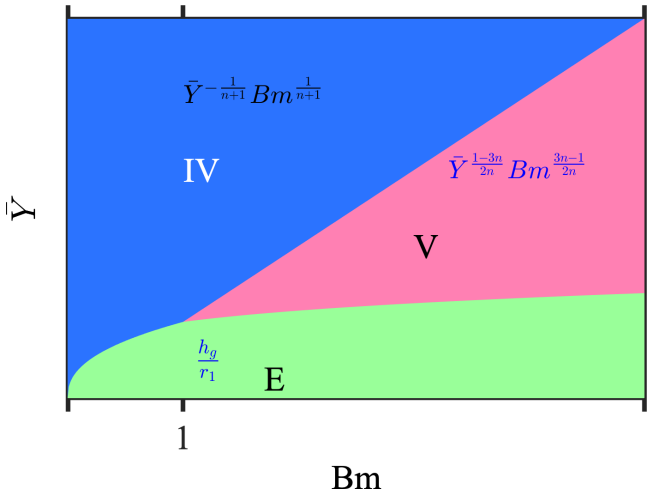

FIG. 5. Asymptotic limits of the reservoir-flow coating thickness Co (blue or black) in absence of surface tension. The parameter space can be divided up into three domains (IV, V, E). The boundary between region IV and V corresponds to $\bar{\mathrm{Y}} = \mathrm{Bm}$, the boundary between IV and E is given by $\bar{\mathrm{Y}} = \mathrm{Bm}^{\frac{1}{2+n}}$, and the boundaries between E and V are given by $\bar{\mathrm{Y}} = \mathrm{Bm}^{(3n-1)/(5n-1)}$ and $\mathrm{Bm} = 1$.

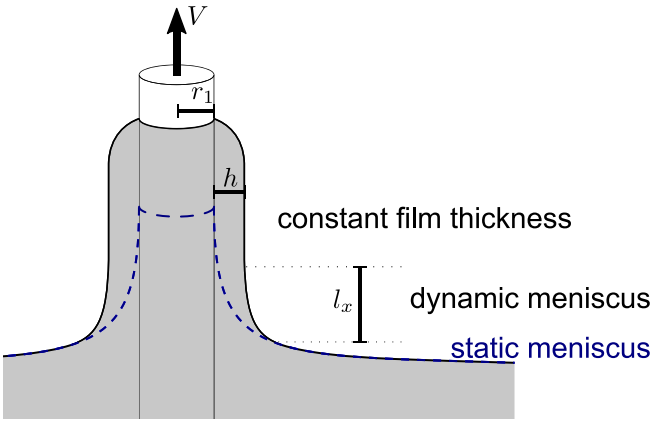

FIG. 6. The meniscus around a rod of radius r_1. The shape of the static meniscus that forms between the rod and the bath at rest is indicated by the blue dashed line. When the rod is withdrawn from the bath, a coating of thickness h is formed. l_x is the length of the dynamic meniscus, which marks the transition between the static meniscus and the coating film.

This region spans over the whole range of B but is limited to low $\bar{\mathrm{Y}}$ values for high Bm values. Writing that $h = h^*$ at the boundaries IV–E and V–E, we find that the analytical expressions of these boundaries are $\bar{\mathrm{Y}} = \mathrm{Bm}^{1/(2+n)}$ and $\bar{\mathrm{Y}} = \mathrm{Bm}^{(3n-1)/(5n-1)}$, respectively.

IV. COATING DRIVEN BY THE MENISCUS FLOW

In this section we assume that the flow in the reservoir drags a sufficient amount of liquid such that the thickness of deposit is fixed by the flow at the level of the meniscus. This regime is observed in situations where the yield stress is small and plays little role. We use dimensional analysis and scaling arguments starting from reasonable physical assumptions in order to obtain scaling laws for the coating thickness. A full numerical calculation of the flows goes beyond the scope of this work.

When a rod is immersed in a reservoir filled with a wetting liquid, a meniscus forms along the rod. Surface tension, gravity, and yield stress are responsible for the deformation of the interface and the shape of the meniscus. A flat horizontal surface is imposed by gravity at distances far away from the rod. In situations of complete wetting, the contact angle between the solid rod and the liquid vanishes. Both constraints are satisfied by bending the interface with a curvature $1/R$, such that the increase of elastic energy stored in the material $\tau_c R^3$ and the increase of the gravitational energy $\rho g R^4$ are compensated by the decrease of surface energy ΓR^2. When the rod is moved upwards, liquid is dragged along. The viscous force is the driving force of the liquid upward motion, whereas surface tension and gravity oppose the fluid motion.

Far from the static meniscus, the film is homogeneous and has a constant thickness. There is always a solid layer at the free surface of the film if the fluid has a finite yield stress. The pressure in the film is lower than in the meniscus. There is therefore a pressure gradient over a characteristic length l_x which is the height of what we call the dynamic meniscus that connects the constant film thickness to the static meniscus; see Fig. 6. The momentum balance equations in the static and dynamic menisci allow us to calculate the height l_x of the dynamic meniscus as well as the thickness of deposit in various limiting situations.

The characteristic parameters involved in the flow are the thickness of deposit h, the radius of the rod r_1, the radius of the reservoir r_2, the gravitational forces by unit volume ρg, the withdrawal velocity of the rod V, the viscous stress τ, and the interfacial tension Γ. These seven parameters involve three fundamental units and, according to the Buckingham's π theorem, a set of four dimensionless parameters are required to describe the flow: We choose the confining parameter Co,

the capillary number for complex fluids $\mathrm{Ca}_f = r_1 k V^n/(\Gamma r_1^n)$ (the ratio between the viscous forces and the surface tension forces with Γ the surface tension), and l_c/r_1 (the ratio of the capillary length divided by the radius of the rod). The capillary length $l_c = \sqrt{\Gamma/(\rho g)}$ measures the importance of gravity. Gravity plays a role if the capillary length l_c is smaller than the radius r_2 of the external wall of the reservoir. We also introduce the yield number $Y = \tau_c r_1/\Gamma$ that compares the yield stress and the capillary stress. In this section we study the limit of small yield stress. These dimensionless numbers are different from and more numerous than those chosen in the previous paragraph. They are more numerous because the surface tension must taken into account in the meniscus. They are different by choice and for convenience in this limit where the yield stress does not play any important role. Indeed, it is important to note that $\mathrm{Ca}_f = \mathrm{Bm}^{-1} Y \mathrm{Co}^n$, and $Y = \bar{Y} r_1^2/l_c^2$. So one might as well choose Co, Bm, l_c/r_1 and $\bar{Y}$ to describe the process. We follow here the choice usually done in literature for power-law fluids. We anticipate that in order to study the transition to the situation where the coating is dominated by the flow in the reservoir studied in Sec. II, we will have to use the same dimensionless parameters in the two limits. In the last section we decide to convert our results in terms of the first set of dimensionless parameters Co, Bm, $\bar{Y}$ into Co, Ca_f, Y, l_c/r_1.

The force balance equation of a liquid slice of thickness dz at a height z is

$$r\tau_{rz}(r) = \left(\rho g + \frac{\partial P}{\partial z}\right)\left[\frac{r^2}{2} - \frac{(r_1+h)^2}{2}\right]. \tag{25}$$

The pressure gradient is obtained from Laplace's law at the surface of the film,

$$\frac{\partial P}{\partial z} = \frac{\partial \mathcal{H}}{\partial z}, \tag{26}$$

where $\mathcal{H}$ is the local curvature of the meniscus. In the dynamic meniscus and at the tip of the static meniscus, the outer surface of the film is very close to a cylinder of radius $r_1 + h$ and $\mathcal{H} = \Gamma/(r_1+h) - \Gamma\partial^2 h/\partial^2 z$. The shear stress at the surface of the rod is given by the Herschel-Bulkley model $\tau_{rz}(r_1) = -\tau_c - k\dot{\gamma}^n$ if $\tau_{rz}(r) < -\tau_c$ and $\tau_{rz}(r_1) = -\beta\tau_c$ if $\tau_{rz}(r) > -\tau_c$ with $0 < \beta < 1$. For a Newtonian or a power-law fluid the yield stress vanishes. In the static meniscus the viscous shear stress close to the wall is negligible by definition. In the yield-stress fluid situation, since the fluid flows in the static meniscus, the shear stress at the wall is less or equal to $-\tau_c$ depending upon the history of the fluid. As the sample close to the wall comes from the reservoir where it was flowing, we assume that it has accumulated a maximal elastic strain so that the shear stress is $\tau_{rz}(r_1) = -\tau_c$.

Depending on the relative values of gravity, viscous force, elasticity, and surface tension terms, different limiting regimes can be obtained. Our method is to study independently all these regimes by focusing on limiting cases where the process is ruled by one or two phenomena. At first glance, this study may look like a multitude of regimes, but in fact it is the only way to deal with the problem at the level of dimensional analysis. The difficulty of this approach does not lie in the resolution of each regime but in their choice and in the way they are connected. The choice of the limiting regimes is based on the set of dimensionless parameters chosen above. The crossovers between regimes are made by equating the ratios of the different forces at the crossover.

In a first step, we neglect the yield stress compared to capillary forces and viscous forces, and we therefore consider a power-law fluid. Then we consider the opposite situation where the yield stress is higher than the capillary forces and the viscous forces. We bridge the two situations by writing that at the boundary the yield-stress force is on the order of the magnitude of the capillary forces. We anticipate that the comparison between yield stress and capillary or viscous stresses are not independent due to the similarity of the equation in the static meniscus and in the dynamic one. The assumption that the yield stress is higher than the capillary stresses but lower than the viscous stresses or the assumptions that the yield stress is higher than the viscous stresses but lower than the capillary stresses do not lead to a solution.

A. Power-law fluid

We consider a power-law fluid with a vanishing yield stress, i.e., $Y = 0$ in the wide reservoir and narrow reservoir geometries. This corresponds to a situation where the fluid in the meniscus is mainly liquid, i.e., there is only a small solid crust at the interface between air and fluid, which plays a negligible role. Based on these limiting behaviors we then propose a phase diagram in the parameter plane $\{\mathrm{Ca}_f, \mathrm{Co}\}$ that summarizes the different behaviors and display the boundaries between them. To analyze this behavior we split the study into several regimes. As said previously, the following should not be seen as a series of special cases. They are in fact the set of limiting situations of the problem that can be analyzed because of the dimensionless numbers that exist in the analysis.

1. Coating from a wide reservoir in the absence of gravity

We first focus on a situation where the gap between the rod and the outer wall of the reservoir is wide ($r_2 > r_1$) and where we can neglect gravity. This situation has been described at length in many work [23–25]. For the sake of clarity and consistency, we recall here the basis and assumptions of these descriptions. In this situation, the force balance from Eq. (25) becomes

$$\frac{\partial P}{\partial z} = \frac{\partial \mathcal{H}}{\partial z} = 0. \tag{27}$$

This leads to $l_x = \sqrt{h(r_1 + h)}$. Assuming that in the dynamics meniscus at the scaling level $\dot{\gamma} \sim V/h$, we then obtain the following scaling laws:

$$\frac{h}{r_1} \simeq \begin{cases} \mathrm{Ca}_f^{\frac{2}{1+2n}} & \text{if} \quad h \ll r_1 \\ \mathrm{Ca}_f^{\frac{1}{n}} & \text{if} \quad h \gg r_1 \end{cases}. \tag{28}$$

The numerical prefactors could in principle be calculated from a full calculation using the method of matched asymptotic expansions [23–25].

2. Coating from a wide reservoir in the presence of gravity

Gravity plays a role if the capillary length l_c is smaller than the radius r_2 of the external wall of the reservoir. When the relevant length scale of the experiment is larger than the capillary length, gravitational forces dominate over capillary forces. In this case we can neglect surface tension and the balance equation of the momentum in the dynamic meniscus writes [see Eq. (24)]

$$-kr_1\left(\frac{V}{h}\right)^n \simeq \frac{\rho g}{2}\left[r_1^2 - (r_1 + h)^2\right], \tag{29}$$

which leads to the thickness of the coating film

$$\frac{h}{r_1} \simeq \begin{cases} \mathrm{Ca}_f^{\frac{1}{1+n}} \left(\frac{l_c}{r_1}\right)^{\frac{2}{1+n}} & \text{if} \quad h \ll r_1 \\ \mathrm{Ca}_f^{\frac{1}{2+n}} \left(\frac{l_c}{r_1}\right)^{\frac{2}{2+n}} & \text{if} \quad h \gg r_1 \end{cases}. \tag{30}$$

3. Coating from a narrow reservoir

If the reservoir is very narrow, i.e., $r_2 - r_1 \leqslant r_1$, the thickness of deposit is small compared to the rod radius, and it is too small for gravity to play a role. The static meniscus has in this limit a toroidal shape of radius $r_2 - r_1$. The momentum balance equations in the static and dynamic menisci lead to $l_x = \sqrt{h(r_2 - r_1)}$ and $\Gamma h^2/l_x^3 = k(V/h)^n$. The thickness of the coating film is then

$$\frac{h}{r_1} \simeq \mathrm{Ca}_f^{\frac{2}{1+2n}} \mathrm{Co}^{\frac{3}{1+2n}}. \tag{31}$$

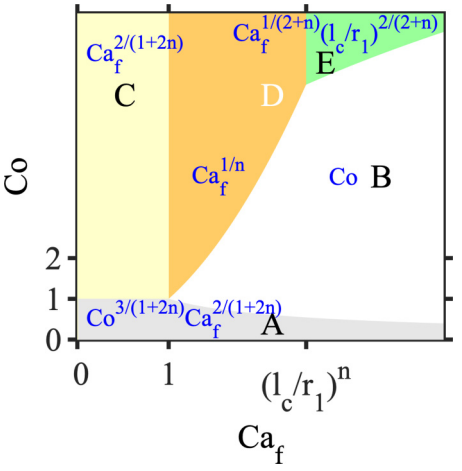

FIG. 7. Asymptotic limits of the meniscus-driven coating thickness h/r_1 (blue). The parameter space can be divided up into domains A–E. The diagram corresponds to $n = 0.5$ and $l_c/r_1 = 6.25$.

Note that when the velocity becomes too large, i.e., $\mathrm{Ca}_f > \mathrm{Co}^{n-1}$, the thickness h becomes of the order of the gap size $r_2 - r_1$.

4. Thickness of the coating film driven by the meniscus flow

We summarize the results of this section on the coating of power-law fluids by a diagram showing the various scaling regimes in the plane of the two relevant dimensionless numbers Ca_f and Co. Figure 7 corresponds to $l_c/r_1 = 6.25$.

For $Y = 0$, $n = 1$ and $\mathrm{Ca}_f < 1$, we find the laws of Landau and Levich [6,7] for Newtonian fluids. We have simply extended the phase diagram to confined geometries. It is important to note that we have not taken into account here the normal stress differences that may be present in these systems. We find a region where the thickness of the deposit varies as $\mathrm{Ca}_f^{1/n}$. This region only exists if the capillary length is greater than the fiber radius (see Fig. 8). This point was not considered

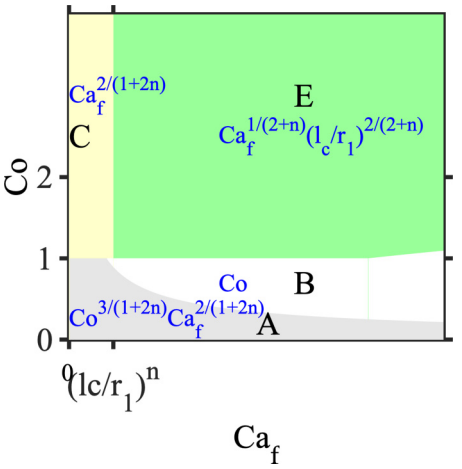

FIG. 8. Asymptotic limits of the meniscus-driven coating thickness h/r_1 (blue). The parameter space can be divided up into domains A–E. This diagram corresponds to $n = 0.5$ and $l_c/r_1 = 0.5$.

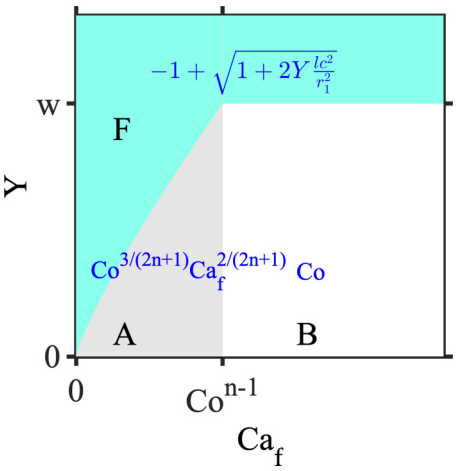

FIG. 9. Asymptotic scaling limits of the meniscus-driven coating thickness h/r_1 (blue). The parameter space can be divided into three domains: A, B, and F. The diagram corresponds to $n = 0.7$, $\mathrm{Co} = 0.1$, and $l_c/r_1 = 1.5$. $w = \frac{[(Co+1)^2-1]r_1^2}{l_c^2}$.

previously. The exponent $1/n$ comes from the fact that we have considered that l_x varies when h becomes larger than r_1. We do not find the divergence proposed by White and Tallmadge for capillary numbers between 1 and l_c/r_1. The divergence proposed by White and Tallmadge [26] results from a perturbative treatment of gravity. It does not seem to be observed experimentally. The boundaries between the regions A–C, A–D, A–B, and B–E are found by imposing the continuity of the thickness in the transition regions: The thickness of deposit in region A is equal to $h/r_1 = \mathrm{Co}^{3/(1+2n)}\mathrm{Ca}_f^{2/(1+2n)}$. The thickness of deposit in region C is equal to $h/r_1 = \mathrm{Ca}_f^{2/(1+2n)}$ for $\mathrm{Ca}_f < 1$. Writing the continuity of coating thickness over regions A and C, yields that the equation of the A–C boundary equals $\{\mathrm{Co} = 1, \mathrm{Ca}_f < 1\}$. Following the same approach we find that the A–B boundary is given by $\{\mathrm{Ca}_f > 1, \mathrm{Co} = \mathrm{Ca}_f^{n-1}\}$, the B–D boundary by $\{1 < \mathrm{Ca}_f < (l_c/r_1)^n, \mathrm{Co} = \mathrm{Ca}_f^{1/n}\}$, and the B–E boundary by $\{(l_c/r_1)^n < \mathrm{Ca}_f, \mathrm{Co} = \mathrm{Ca}_f^{1/(2+n)}(l_c/r_1)^{2/(2+n)}\}$.

To conclude this section, Fig. 8 displays the same situation for $l_c/r_1 = 0.5$.The boundaries between the different regions are determined following the same rules above. Note that the region D does not exist if the radius of the rod r_1 is larger than the capillary length l_c and that the equations determining the boundaries between the various regions depend upon n, l_c/r_1, and Co.

B. Coating by a fluid with a finite yield stress

If the yield-stress value is high compared to the stress created by the surface tension and to the viscous stresses, the sample behaves as a gel. The static and dynamic menisci are jammed. In this context, the coating process can be assimilated to a fracture process. It is not possible to find a scaling law by analyzing the momentum equations in the static and dynamic meniscus as previously: Both lead to the same relationship. It is possible only to give an upper value of the film thickness in the flat zone by imposing that the system be jammed, i.e. that the stress be equal to the yield-stress value at the level of the rod. We get

$$\frac{h}{r_1} = -1 + \sqrt{1 + 2Y\frac{l_c^2}{r_1^2}}. \tag{32}$$

This equation is valid both for wide and narrow reservoirs.

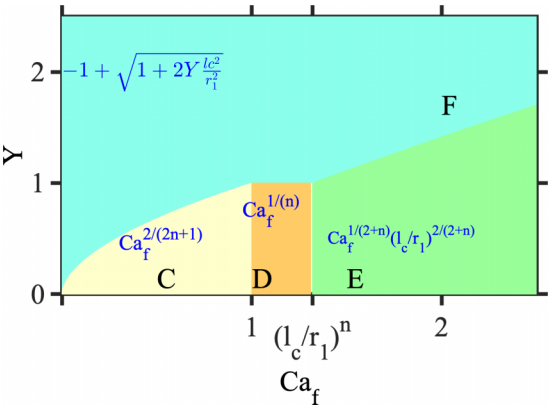

FIG. 10. Asymptotic scaling limits of the meniscus-driven coating thickness in very wide geometry for $n = 0.4$, $l_c/r_1 = 2$, and $\mathrm{Co} = 10$ (h/r_1 in blue).

C. Review of the different regimes when the thickness of deposit is driven by the meniscus

To summarize these results, we display in Figs. 9 and 10 the predicted regimes for the film thickness in the parameter plane $\{\mathrm{Ca}_f, Y\}$ when the thickness of deposit is driven by the flow in the meniscus. As said above, to set the cross over between the power-law fluid and the yield-stress fluid, we consider that the power-law fluid corresponds to the situation where the yield-stress is negligible with respect to viscous loss. In other words, the power-law fluid behavior describes the case of a meniscus bearing only a very thin layer of jammed fluid located close to the air-fluid interface.

Let us now consider the regimes C and F. Regime C is valid if we can neglect the yield stress with respect to the viscous dissipation. At the boundary between the two regimes, both terms are equal. This gives

$$\tau_c = k\left(\frac{V}{h}\right)^n, \tag{33}$$

$$\frac{h}{r_1} = \mathrm{Ca}_f^{\frac{2}{1+2n}}. \tag{34}$$

The boundary between the regimes C and F is given by $Y = \mathrm{Ca}_f^{1/(1+2n)}$. In region C, $h/r_1 = \mathrm{Ca}_f^{2/(1+2n)}$ and in region F, $h/r_1 = Y l_c^2/r_1^2$. Using the same procedure, the D–F boundary is given by $Y = 1$, and the E–F boundary is given by $Y = (r_1/l_c)^{2n/(1+2n)}\mathrm{Ca}_f^{(1+n)/(1+2n)}$. In region D, the coating thickness scales as $h/r_1 = \mathrm{Ca}_f^{1/n}$. The boundaries between regions C, D, and E are set by imposing the continuity of the h value: The C–D boundary writes $\mathrm{Ca}_f = 1$ and the D–E boundary corresponds to $h = l_c$ and writes $\mathrm{Ca}_f = (l_c/r_1)^{1/n}$. Figures 9 and 10 evidence a zone for large Y value where the thickness of deposit is governed by a competition between gravitational stresses and the yield stress. A simple image emerges from this analysis, when $Y > 1$ for low capillary number, the sample is jammed in the meniscus and the thickness is given by a balance between gravity stresses and yield stress.

V. COATING DIAGRAM

In this section, we put together the results of the two previous sections and specify the cases in which the thickness of the deposited film is controlled by the flow in the meniscus and those in which it is controlled by the flow in the reservoir. Our aim is to combine Fig. 5 and Fig. 10 into a single general diagram, which presents the possible regimes for the coating thickness as a function of the yield number Y and the capillary number Ca_f for fixed values of the confinement parameter

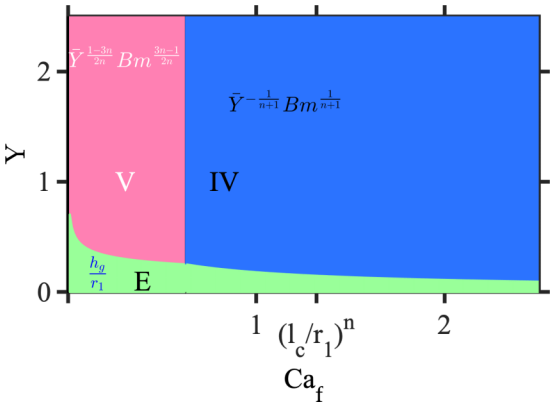

FIG. 11. The equivalent of Fig. 5 in the parameter plane $\{Y, \mathrm{Ca}_f\}$.

Co and of l_c/r_1. We focus on the case of large reservoirs. Fig. 5 uses the variables $\bar{Y}$ and Bm and Fig. 10 the variables Y and Ca_f. Some transition lines are obtained as functions of the ratio l_c/r_1 of the capillary length to the radius of the rod. It is straightforward to transpose Fig. 5 into the variables of Fig. 10. We recall that $\mathrm{Ca}_f = \mathrm{Bm}^{-1} Y \mathrm{Co}^n$, and $Y = \bar{Y} r_1^2/l_c^2$. The boundary between zone V and zone IV is $\mathrm{Ca}_f^* = \mathrm{Co}^n r_1^2/l_c^2$. Zone V corresponds to small Ca_f values. Zone E for $\mathrm{Ca}_f < \mathrm{Ca}_f^*$ ranges from $Y = 0$ to $Y = \mathrm{Co}^{(3n-1)/2} \mathrm{Ca}_f^{(1-3n)/2n} (r_1/l_c)^{(5n-1)/n}$ and for $\mathrm{Ca}_f > \mathrm{Ca}_f^*$ extends from $Y = 0$ to $Y = \mathrm{Co}^{n/(1+n)} \mathrm{Ca}_f^{-1/(1+n)} (r_1/l_c)^{(4+2n)/(1+n)}$. To find at every point of the parameter plane $\{\mathrm{Ca}_f, Y\}$ the deposit thickness, we compare the expressions found in Figs. 10 and 11.

The measured deposit thickness is the thickness dictated by the limiting phenomenon, i.e., the thinnest thickness. We anticipate that this construction depends upon the values of Co and of l_c/r_1. We applied this construction rule to build Fig. 12. Although this criterion is simple, the detailed analysis of the different cases is rather tedious. Instead, we prefer to draw a complete diagram in the parameter plane $\{Y, \mathrm{Ca}_f\}$.

Figure 12 displays the results for the thickness of the coating film deposited from very large reservoirs. Regions C, D, and E correspond at high capillary numbers to a limit where the deposit thickness is limited by the flow in the liquid meniscus and to the behavior of fluids with very low yield stress. As the capillary number increases, the thickness of deposit increases and drainage and gravity play any role for $\mathrm{Ca}_f > (l_c/r_1)^n$. In regions IV and V, the material supply to the film is

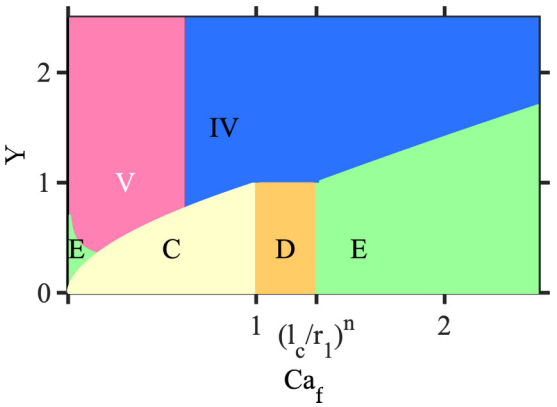

FIG. 12. Coating diagram in the parameter plane $\{Y, \mathrm{Ca}_f\}$ for $l_c/r_1 = 2$, $\mathrm{Co} = 10$, and $n = 0.4$.

TABLE I. Rheological characteristics of the Carbopol gels used in the dip-coating experiments. The rheological parameters are obtained using a Discovery HR-2 rheometer (TA Instruments) in a parallel-plate geometry with a gap size of 1 mm. The parameters τ_c, k, and n are obtained by fitting the flow curve (shear stress versus shear rate) by the Herschel-Bulkley model and correcting for the inhomogeneous shear rate in the parallel-plate geometry [27]. The value of the surface tension Γ has been reported by Jørgensen and co-workers [28]. For sample 4, a lower value is obtained by addition of 1% aqueous PEG-12 dimethicone (detailed in Ref. [13]). The viscoelastic properties are determined by imposing an oscillatory strain comprising between 0.1%–100% at a frequency of 1 Hz. The storage modulus G is then obtained by averaging over the linear viscoelastic regime between 0.1%–3%.

Sample number	τ_c (Pa)	k (Pa s^n)	n	Γ (mN/m)	G (Pa)
1	3.0	1.6	0.47	63	24
2	27.6	14.4	0.35	63	237
3	69.0	29.6	0.35	63	450
4	53.6	28.7	0.35	27	385

limited by the flows in the reservoir, which means that neither gravity nor capillarity play role in the thickness of the deposited film. In region E at low capillary number, the thickness of deposit results from a competition between the amount of liquid given by the reservoir and gravity. Note that in the situation where $l_c < r_1$, zone D disappears, but the diagram remains roughly the same. From this diagram, the following simple picture emerges: When $Y > 1$ (i.e., when the yield stress exceeds the Laplace pressure), the thickness of deposit is governed by the flow inside the reservoir. The deposit thickness h varies as a function of the capillary number. When $Y < 1$, the situation is more complex and h depends on the geometry as well as upon the capillary number.

VI. COMPARISON WITH EXPERIMENT

Here we compare some theoretical predictions with our previous experimental data [13] and additional experiments following the same protocol. The dip-coating experiments are carried out with Carbopol gels of yield stress $\tau_c = 3$–69 Pa (see Table I). Acrylic rods of radius $r_1 = 2.5$, 5, and 10 mm are immersed over a height of $H = 10$ cm into a reservoir of radius ranging from $r_2 = 13$ to 33 mm. Next, the rods are vertically withdrawn with velocity $V = 0.1$–10 mm/s giving rise to Bingham numbers between 2 and 10. The thickness profile of the coating films is directly measured

TABLE II. Comparison of the thickness of the deposit predicted by the bath-flow model and from experiment with $r_2 = 33$ mm for the samples in Table I and a withdrawal velocity of $V = 3$ mm/s.

Sample number	r_1 (mm)	Bm	Y	h_{exp} (mm)	h_{th} (mm)
1	2.5	5.6	0.1	0.18 ± 0.02	0.49
	5	5.4	0.2	0.20 ± 0.02	0.69
	10	4.9	0.5	0.26 ± 0.01	0.85
2	2.5	4.3	1.1	0.31 ± 0.01	0.36
	5	4.2	2.2	0.59 ± 0.02	0.53
	10	3.9	4.4	0.71 ± 0.09	0.67
3	2.5	5.2	2.7	0.29 ± 0.03	0.32
	5	5.1	5.5	0.58 ± 0.04	0.47
	10	4.8	11	0.72 ± 0.07	0.60
4	2.5	4.2	5.0	0.33 ± 0.04	0.36
	5	4.1	9.9	0.51 ± 0.03	0.53
	10	3.8	20	0.68 ± 0.03	0.68

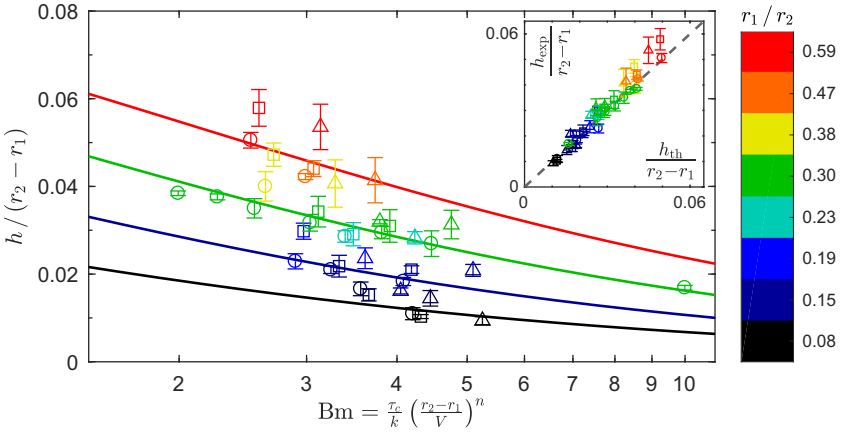

FIG. 13. Steady coating thickness for different ratio r_1/r_2 (color coding in legend) as a function of Bingham number Bm for Carbopol gels of $\tau_c = 28$ Pa (sample 2, squares), $\tau_c = 54$ Pa (sample 4, circles), and $\tau_c = 67$ Pa (sample 3, triangles). The theoretical predictions (solid lines) follow from calculations of the flow inside the bath. Inset: normalized theoretical coating thickness h_{th} versus experimental values h_{exp}.

using a Keyence LJ-V7060K profilometer. The experimental conditions are such that a steady flow is reached and a constant coating thickness can be determined.

For each experiment, the material parameters of the gels are reported in Table I. A selection of the experimentally determined coating thickness is reported in Table II. The values are given for the widest bath under scrutiny ($r_2 = 33$ mm) and a withdrawal velocity of $V = 3$ m/s. For samples 2–4 of relatively high yield stress and $Y \equiv \tau_c r_1/\Gamma > 1$, the experimental values are well described and within 20% of the predictions by the bath-flow model. For sample 1 with $Y < 1$, a discrepancy of a factor of ~3 is observed. This shows that for $Y < 1$, the thickness is ruled by the flow in the meniscus and not by the flow inside the bath.

A comparison between the experimental data for $Y > 1$ and the bath-flow model is given in Fig. 13. The experimental observations are well described by the bath model over the full range of the explored parameter space of $\mathrm{Bm} \in [2, 10]$ and $r_1/r_2 \in [0.08, 0.59]$.

As expected, when $Y < 1$, the experimental observations are not in agreement with the bath-flow model.

VII. CONCLUDING REMARKS

We have studied the withdrawal of a rod from a yield-stress fluid reservoir. The coating layer is formed in the meniscus region, where the yield-stress fluid progressively crosses over from a liquid to a solid behavior. For the cylindrical geometry under current scrutiny, symmetry allows for a semianalytical determination of the stress field inside the reservoir from the velocity boundary conditions and mass conservation. Our results show that the thickness of the coating layer can be controlled by selecting the size of the reservoir and the pull-out velocity.

The semianalytic model and the scaling laws presented here provide a guide to control the coating thickness and to optimize performance and costs in industrial applications. Depending upon the yield stress, surface tension, and geometry, the thickness of deposit may be controlled either by the flow in the reservoir or by the flow in the meniscus. A simple image emerges from our calculations. If the dimensionless number $Y = \tau_c r_1/\Gamma$ is greater than one, the thickness of deposit is governed by the flow inside the reservoir whatever the geometry and the capillary number. A comparison of the coating thickness predicted by Eq. (20) with experimental observations shows a good agreement in the limit where the yield number Y is larger than one. The semianalytic model and the scaling

laws also suggest for instance that the use of surfactants has no impact on the thickness of deposit for high value of the yield stress. In the case of an eccentric configuration of rod and bath or a total absence of cylindrical symmetry, the coating thickness may be inhomogeneous. In these cases, we recommend the use of a large bath to obtain the most homogeneous coating layer.

To conclude, let us summarize the main hypothesis of this work and propose some perspectives. We have proposed scaling laws for the thickness of deposit when the flow is governed by the reservoir or by the meniscus. These scaling laws have to be used in their range of validity. Our description is weak when the flow is governed by what happens in the meniscus and when the meniscus is solid. In this last situation, the coating process corresponds to a fracture process, and we are simply able to give an upper bound of the thickness.

This work is restricted to a steady flow. We have shown that a steady flow is achieved when the time of the experiment is larger than the time required to reach a steady shear stress profile. As shown in our previous work [13], this occurs in many experimental configurations as soon as the gap between the rod and the external reservoir is not too wide. The extension of this work to transient regimes is more complex and requires numerical work to describe both the elastic and fluid behaviors. We believe that the use of a nonlocal model [29,30] is necessary to take into account the appearance of shear bands.

We also have neglected normal stresses in Eq. (3). Usually yield-stress fluids exhibit low normal stresses compared to polymer solutions [31]. Bonn and co-workers have shown that in those systems the second normal stress difference N_2 is negligible compared to the first normal stress differences N_1 which scales as $N_1 \propto \tau^2/G$ [32] where τ is the stress and G the shear modulus. Our hypothesis requires that $N_1 R \ll \Gamma$ where R is the meniscus curvature. Assuming $\tau_c = G\gamma_c$ with γ_c the yield strain the criterion writes $\tau_c \gamma_c R \ll \Gamma$. In a standard situation ($R = 2$ mm, $\Gamma = 63$ mN/m, $\gamma_c = 0.1$), this hypothesis is valid for gels with a yield stress less than $\sim$300 Pa.

Last but not the least, instabilities such as viscous fingering or Rayleigh Plateau instabilities may occur when the rod is withdrawn from the reservoir. We have not included these phenomena in our description.

The main perspective of this work concerns the experimental testing of the scaling laws. As stated above, the experiments in the literature are in agreement with the predicted flow diagram but do not constitute a quantitative test for it. Experiments with samples of small yield stress and on a large range of capillary numbers are necessary for an accurate test of the flow diagram.

ACKNOWLEDGMENTS

W.J.S. acknowledges funding from the People Programme (Marie Curie Actions) of the European Union's Seventh Framework Programme (FP7/2007-2013) under REA grant agreement n. PCOFUND-GA-2013-609102, through the PRESTIGE program coordinated by Campus France.

APPENDIX A: EXISTENCE OF A STEADY FLOW

Saramito has proposed an elastoviscoplastic model [20,33] which has the advantage to be tensorial and simple. The constitutive equation of this model reads [20]

$$\frac{\overset{\square}{\boldsymbol{\tau}}}{G} + \max\left(0, \frac{|\boldsymbol{\tau}| - \tau_c}{k}\right)^{\frac{1}{n}} \frac{\boldsymbol{\tau}}{|\boldsymbol{\tau}|} = \dot{\gamma}, \tag{A1}$$

where G is the elastic modulus, $\dot{\gamma}$ is the shear rate, and $\overset{\square}{\tau}$ is the Gordon-Schowalter convected time derivative of the stress tensor, defined by [34,35]

$$\overset{\square}{\boldsymbol{\tau}} = \dot{\boldsymbol{\tau}} + \mathbf{v}\cdot\nabla\boldsymbol{\tau} + \boldsymbol{\tau}W(\mathbf{v}) - W(\mathbf{v})\boldsymbol{\tau} - a(\boldsymbol{\tau}D(\mathbf{v}) + D(\mathbf{v})\boldsymbol{\tau}) \tag{A2}$$

with $W(\mathbf{v}) = (\nabla\mathbf{v} - \nabla\mathbf{v}^{\mathsf{T}})/2$ the vorticity tensor, $D(\mathbf{v}) = (\nabla\mathbf{v} + \nabla\mathbf{v}^{\mathsf{T}})/2$ the rate of deformation tensor, and the interpolation parameter is such that $|a| \leqslant 1$ [33]. The vertical withdrawal of a rod

from the reservoir gives rise to a vertical flow in the fluid regions away from the meniscus and the end of the rod [Fig. 2(a)]. The only nonvanishing stress component is the shear stress τ_{rz}, and the only nonvanishing shear rate component is the shear rate $\dot{\gamma}_{rz}$. For $a = 1$, the temporal evolution of τ_{rz} writes

$$\dot{\gamma}_{rz} = \frac{1}{G}\frac{\partial \tau_{rz}}{\partial t} + \max\left(0, \frac{|\tau_{rz}| - \tau_c}{k^n}\right)^{\frac{1}{n}} \frac{\tau_{rz}}{|\tau_{rz}|}. \tag{A3}$$

When $\tau_{rz}(r) \leqslant \tau_c$, Eq. (A3) reduces to the Kelvin-Voigt model for a elastic solid. The characteristic time T of the dynamics of the velocity profile of the gel for stresses values higher than the yield stress is given by $T = \tau_c/(G\dot{\gamma})$ with G the elastic modulus. The sheared band close to the wall of the reservoir involves the longest characteristic time which is equal to $\tau_c(r_2 - \lambda_o)/(GV_d)$, where V_d is the downward velocity of the fluid and λ_o is the position in the reservoir where the stress is equal to $+\tau_c$. Neglecting the wetting film on the external wall which is much smaller than the film thickness h, mass conservation gives $V_d = -V(r_1 + h)^2/(r_2^2 - r_1^2)$ where V is the velocity of the rod. In the main text we consider situations where $T_{\text{exp}} > T$ and assume a steady flow. In this situation the Saramito model [Eq. (A3)] reduces to the Herschel-Bulkley model [Eq. (2)].

APPENDIX B: ASYMPTOTIC POWER LAWS FOR THE RESERVOIR-FLOW MODEL

When the Bingham number and r_1/r_2 take extreme values, it is possible to derive asymptotic scaling laws for the inner yield location λ_i and the coating thickness h. Five cases can be distinguished. First, we treat the limits of fast withdrawal corresponding to small Bingham number (I–II). Second, we treat the cases of large Bingham number (III–V).

1. Small Bingham number

When the withdrawal velocity is large and $V(k/\tau_c)^{\frac{1}{n}} \gg r_2 - r_1$ (Bm $\ll 1$), the yield locations λ_i and λ_o tend to the same value λ_*, which can be found by solving Eq. (18). Substitution of $p = 1 - r^2/\lambda_*^2$ on the left-hand side and of $p = -1 + r^2/\lambda_*^2$ on the right-hand side of Eq. (18) gives

$$\int_0^{1-\frac{r_1^2}{\lambda_*^2}} (1-\rho)^{\frac{1}{2}-\frac{1}{2n}} p^{\frac{1}{n}}\, dp = \int_0^{\frac{r_2^2}{\lambda_*^2}-1} (1+\rho)^{\frac{1}{2}-\frac{1}{2n}} p^{\frac{1}{n}}\, dp. \tag{B1}$$

This equation can be solved for λ_* numerically. Note that the value of λ_* depends neither on the yield stress τ_c nor on the consistency k but solely on the power index n and the geometrical parameters r_1 and r_2.

In the special case of $n = 1$ (Bingham fluid), the solution to Eq. (B1) is given by

$$\lambda_* = \sqrt{\frac{r_1^2 + r_2^2}{2}}, \tag{B2}$$

and the coating thickness can be calculated using Eq. (21):

$$h = -r_1 + \frac{r_2^2 - r_1^2}{2\sqrt{\left(r_1^2 + r_2^2\right)\ln\left(\frac{1}{2} + \frac{r_2^2}{2r_1^2}\right) + r_1^2 - r_2^2}}. \tag{B3}$$

λ_* approaches λ_i within 20% for Bm $\leqslant 0.3$ and $r_1 = 0.1\, r_1$, for Bm $\leqslant 1$ and $r_1 = 0.5\, r_1$, and for Bm $\leqslant 8$ and $r_1 = 0.9\, r_1$ (see dotted lines in Fig. 3).

I. Small gap

When the channel width $r_2 - r_1$ is small with respect to r_1, the values for p in Eq. (B1) are small. A first-order expansion yields the following scaling-law approximation for any n:

$$\lambda_* \simeq \frac{r_1 + r_2}{2} + \frac{n - \frac{1}{4}}{1 + 2n} \frac{(r_2 - r_1)^2}{r_1 + r_2}. \tag{B4}$$

Equation (B4) matches the exact result within 20% for $r_1 \geqslant 0.5\, r_2$, $n \geqslant 0.2$, and $\mathrm{Bm} \leqslant 0.3$ (see dashed lines in Fig. 3). As λ_*/r_1 is close to unity, we can make use of Eq. (22) to obtain the coating thickness

$$h \simeq \frac{n}{2 + 4n}(r_2 - r_1)\left(1 + \frac{4n - 1}{2 + 4n} \frac{r_2 - r_1}{r_1 + r_2}\right). \tag{B5}$$

Note that for small channel widths and large withdrawal velocities, a flow instability similar to viscous fingering is prone to occur [36–41].

II. Large reservoir

When the rod is small with respect to the size of the reservoir ($r_1 \ll r_2$), the ratio r_1/λ_* is small. For $\frac{1}{3} < n < 1$, the left-hand side of Eq. (B1) remains finite for $r_1/\lambda_* \to 0$ and r_2/λ_* converges to a constant. For $n \leqslant \frac{1}{3}$, the left-hand side of Eq. (B1) diverges for $r_1/\lambda_* \to 0$ and the integral is dominated by its upper bound $1 - r_1^2/\lambda_*^2$. The right-hand side of Eq. (B1) is dominated by the upper bound $r_2^2/\lambda_*^2 - 1$. Neglecting the lower bound, one obtains to leading order the power-law relation

$$\lambda_* \propto \begin{cases} \left(\frac{1+3n}{1-3n}\right)^{\frac{n}{2}} r_1^{\frac{1-3n}{2}} r_2^{\frac{1+3n}{2}} & \text{for} \quad 0 < n < \frac{1}{3} \\ \frac{r_2}{\sqrt{\ln \frac{r_2}{r_1}}} & \text{for} \quad n = \frac{1}{3} \\ r_2 & \text{for} \quad \frac{1}{3} < n < 1 \end{cases}. \tag{B6}$$

The coating thickness is imposed by Eq. (20), which can be written as

$$h \simeq \lambda_* \sqrt{\frac{\int_{\frac{r_1}{\lambda_*}}^1 p^{2-\frac{1}{n}}(1-p^2)^{\frac{1}{n}}\, dp}{\int_{\frac{r_1}{\lambda_*}}^1 p^{-\frac{1}{n}}(1-p^2)^{\frac{1}{n}}\, dp}} - r_1. \tag{B7}$$

For $\frac{1}{3} < n < 1$, the integral in the numerator converges for $r_1/\lambda_* \to 0$, whereas the integral in the denominator is dominated by its lower bound. For $n \leqslant \frac{1}{3}$, both integrals are dominated by the lower bound r_1/λ_*. Neglecting the insignificant upper bound, one finds

$$h \propto \begin{cases} r_1\left(\sqrt{\frac{1-n}{1-3n}} - 1\right) & \text{for} \quad 0 < n < \frac{1}{3} \\ r_1\sqrt{\ln \frac{r_2}{r_1}} & \text{for} \quad n = \frac{1}{3} \\ r_1^{\frac{1-n}{2n}} r_2^{-\frac{1-3n}{2n}} & \text{for} \quad \frac{1}{3} < n < 1 \end{cases}. \tag{B8}$$

2. Large Bingham number

We now explore the slow withdrawal limit with $\mathrm{Bm} \gg 1$ and consider two cases.

III. Reservoir with a small gap

When the gap of the reservoir $r_2 - r_1$ is small with respect to the rod radius r_1, λ_i is close to r_1 and λ_o is close to r_2. From the mass conservation condition [Eq. (13)], we infer

$$r_1^2 \int_{r_1}^{\lambda_i} \dot{\gamma}_{rz}(r)\, dr \simeq -r_2^2 \int_{\lambda_o}^{r_2} \dot{\gamma}_{rz}(r)\, dr. \tag{B9}$$

Using this result in the velocity boundary conditions [Eq. (11)] and performing series expansions of λ_i around r_1 and of λ_o around r_2 yields

$$\lambda_i \simeq r_1 + \frac{1}{2}\left(\frac{1+n}{n}\right)^{\frac{n}{1+n}} r_1 \left(\frac{r_2 - r_1}{r_1}\right)^{\frac{1}{1+n}} \mathrm{Bm}^{-\frac{1}{1+n}}. \tag{B10}$$

For $r_1 = 0.9\, r_2$, this expression is within 20% of the exact result for $\mathrm{Bm} \geqslant 41$ and $n = 1$, for $\mathrm{Bm} \geqslant 15$ and $n = 1$, and for $\mathrm{Bm} \geqslant 11$ and $n = 0.2$ (see red dotted-dashed lines in Fig. 3).

From Eq. (22) we obtain the coating thickness

$$h \simeq \frac{r_1}{2+4n}\left[\left(\frac{1+n}{n}\right)^n \frac{r_2 - r_1}{r_1}\right]^{\frac{1}{1+n}} \mathrm{Bm}^{-\frac{1}{1+n}}. \tag{B11}$$

Note that for a given gap size the coating thickness increases with rod size as $h \propto r_1^{\frac{n}{1+n}}$.

IV–V. Reservoir with a large gap

We now treat the case of a large reservoir size with respect to the rod radius, i.e., $r_2 \gg r_1$. For $\mathrm{Bm} \gg 1$, the velocity of the solid region tends to zero and $\lambda_o \to r_2$. We have

$$V \simeq -\int_{r_1}^{\lambda_i} \dot{\gamma}_{rz}(r)\, dr = \left(\frac{\tau_c}{k}\right)^{\frac{1}{n}} \int_{r_1}^{\lambda_i} \left(\frac{\lambda_i}{r} - 1\right)^{\frac{1}{n}} dr. \tag{B12}$$

Employing the variable substitution $p = 1 - r/\lambda_i$ yields

$$V\left(\frac{k}{\tau_c}\right)^{\frac{1}{n}} \simeq \lambda_i \int_0^{1-\frac{r_1}{\lambda_i}} \left(\frac{p}{1-p}\right)^{\frac{1}{n}} dp. \tag{B13}$$

We distinguish two limits:

IV. When $V(k/\tau_c)^{\frac{1}{n}} \ll r_1$, λ_i is close to r_1 and p is small. Performing the first-order expansion $(1-p)^{-\frac{1}{n}} \simeq (1 + p/n)$, we obtain

$$\lambda_i \simeq r_1 + r_1 \left(\frac{1+n}{n}\right)^{\frac{n}{1+n}} \left(\frac{k}{\tau_c}\frac{V^n}{r_1^n}\right)^{\frac{1}{1+n}}. \tag{B14}$$

Note that λ_i is independent on the reservoir radius r_2 and reaches a plateau value when r_2 increases. This contrasts with the findings for a plate geometry, for which the thickness of the liquid region diverges with increasing reservoir size; see Sec. B of the SM [14]. For $r_1 \leqslant 0.1\, r_2$, Eq. (B14) approximates the exact result within 20% for $\mathrm{Bm} \geqslant 0.7$ in the case of $n = 1$, $\mathrm{Bm} \geqslant 1.4$ in case of $n = 0.35$, and for $\mathrm{Bm} \geqslant 3$ in case of $n = 0.2$; see blue dotted-dashed lines in Fig. 3. When drainage and gravity can be neglected, the coating thickness can be calculated using Eq. (22), which gives

$$h \simeq \frac{n r_1}{1+2n}\left(\frac{1+n}{n}\frac{r_2 - r_1}{r_1}\right)^{\frac{n}{1+n}} \mathrm{Bm}^{-\frac{1}{1+n}}. \tag{B15}$$

V. When $V(k/\tau_c)^{\frac{1}{n}} \gg r_1$, r_1/λ_i is small and the integral on the right-hand side of Eq. (B13) is dominated by the upper bound limit for which p is close to unity. Neglecting the lower bound and approximating $\frac{p}{1-p} \approx \frac{1}{1-p}$, we find to leading order

$$\lambda_i \simeq \begin{cases} \left(\frac{1-n}{n}\right)^n r_1^{1-n} \frac{k}{\tau_c} V^n & \text{for} \quad 0 < n < 1 \\ \frac{1}{\ln \frac{kV}{\tau_c r_1}} \frac{kV}{\tau_c} & \text{for} \quad n = 1 \end{cases}. \tag{B16}$$

We would like to stress that the approximations made are rather rough and the approximate value of λ_i may differ substantially from the exact solution, especially for n equal or close to one.

Nevertheless, the power-law relation can be insightful. The coating thickness from Eq. (20) is approximated by

$$h \simeq -r_1 + \lambda_i \sqrt{\frac{\int_{\frac{r_1}{\lambda_i}}^{1} p^{2-\frac{1}{n}}(1-p)^{\frac{1}{n}}\,dp}{\int_{\frac{r_1}{\lambda_i}}^{1}\left(\frac{1}{p}-1\right)^{\frac{1}{n}}\,dp}}. \tag{B17}$$

For $n \leqslant \frac{1}{3}$, both integrals are dominated by the lower bound r_1/λ_i. For $\frac{1}{3} < n \leqslant 1$, the integral in the numerator converges for $r_1/\lambda_* \to 0$, whereas the integral in the denominator is dominated by the lower bound. To leading order, we obtain the power-law dependency

$$h \propto \begin{cases} r_1\left(\sqrt{\frac{1-n}{1-3n}}-1\right) & \text{for} \quad 0 < n < \frac{1}{3} \\ r_1\sqrt{\ln\frac{kV^n}{\tau_c r_1^n}} & \text{for} \quad n = \frac{1}{3} \\ r_1\left(\frac{kV^n}{\tau_c r_1^n}\right)^{-\frac{1-3n}{2n}} & \text{for} \quad \frac{1}{3} < n < 1 \\ \frac{kV}{\tau_c}\frac{1}{\sqrt[3]{\ln\frac{kV}{\tau_c r_1}}} & \text{for} \quad n = 1 \end{cases}. \tag{B18}$$

It is worth mentioning that for large reservoirs, it may take a while until the stress field converges and a steady flow is reached. For a rod of finite length, the transient regime can cover the entire length and the steady flow relations do not apply.

[1] D. Grosso, How to exploit the full potential of the dip-coating process to better control film formation, J. Mater. Chem. **21**, 17033 (2011).

[2] D. Lin and Y. Zhao, Innovations in the development and application of edible coatings for fresh and minimally processed fruits and vegetables, Compr. Rev. Food Sci. Food Saf. **6**, 60 (2007).

[3] C. J. Brinker, G. C. Frye, A. J. Hurd, and C. S. Ashley, Fundamentals of sol–gel dip coating, Thin Solid Films **201**, 97 (1991).

[4] C. J. Brinker, A. J. Hurd, P. R. Schunk, G. C. Frye, and C. S. Ashley, Review of sol-gel thin film formation, J. Non. Cryst. Solids **147–148**, 424 (1992).

[5] P. Innocenzi, *The Sol-to-Gel Transition*, 2nd ed. (Springer, Cham, 2019).

[6] L. Landau and B. Levich, Dragging of a liquid by a moving plate, Acta Physicochim. URSS **17**, 42 (1942).

[7] B. V. C. R. Derjaguin, Thickness of liquid layer adhering to walls of vessels on their emptying and the theory of photo- and motion-picture film coating, CR (Dokl.) Acad. Sci. URSS **39**, 13 (1943).

[8] D. Quéré, Fluid coating on a fiber, Annu. Rev. Fluid Mech. **31**, 347 (1999).

[9] E. Rio and F. Boulogne, Withdrawing a solid from a bath: How much liquid is coated? Adv. Colloid Interface Sci. **247**, 100 (2017).

[10] M. Maillard, J. Boujlel, and P. Coussot, Solid-Solid Transition in Landau-Levich Flow with Soft-Jammed Systems, Phys. Rev. Lett. **112**, 068304 (2014).

[11] M. Maillard, J. Boujlel, and P. Coussot, Flow characteristics around a plate withdrawn from a bath of yield stress fluid, J. Non-Newton. Fluid Mech. **220**, 33 (2015).

[12] M. Maillard, C. Bleyer, A. L. Andrieux, J. Boujlel, and P. Coussot, Dip-coating of yield stress fluids, Phys. Fluids **28**, 053102 (2016).

[13] W. J. Smit, C. Kusina, J.-F. Joanny, and A. Colin, Stress Field Inside the Bath Determines Dip Coating with Yield-Stress Fluids in Cylindrical Geometry, Phys. Rev. Lett. **123**, 148002 (2019).

[14] See Supplemental Material at http://link.aps.org/supplemental/10.1103/PhysRevFluids.6.063302 for a description of the bath flow for a plate. We derived all the equations and solve them in this geometry.

[15] D. Fraggedakis, Y. Dimakopoulos, and J. Tsamopoulos, Yielding the yield stress analysis: A thorough comparison of recently proposed elasto-visco-plastic (EVP) fluid models, J. Non-Newton. Fluid Mech. **236**, 104 (2016).
[16] I. Cheddadi, P. Saramito, C. Raufaste, P. Marmottant, and F. Graner, Numerical modelling of foam Couette flows, Eur. Phys. J. E **27**, 123 (2008).
[17] I. Cheddadi, P. Saramito, B. Dollet, C. Raufaste, and F. Graner, Understanding and predicting viscous, elastic, plastic flows, Eur. Phys. J. E **34**, 1 (2011).
[18] I. Cheddadi, P. Saramito, and F. Graner, Steady Couette flows of elastoviscoplastic fluids are nonunique, J. Rheol. **56**, 213 (2012).
[19] D. Fraggedakis, Y. Dimakopoulos, and J. Tsamopoulos, Yielding the yield-stress analysis: A study focused on the effects of elasticity on the settling of a single spherical particle in simple yield-stress fluids, Soft Matter **12**, 5378 (2016).
[20] P. Saramito, A new elastoviscoplastic model based on the Herschel-Bulkley viscoplastic model, J. Non-Newton. Fluid Mech. **158**, 154 (2009).
[21] A. Fredrickson and R. B. Bird, Non-Newtonian flow in annuli, Ind. Eng. Chem. **50**, 347 (1958).
[22] E. J. Fordham, S. H. Bittleston, and M. A. Tehrani, Viscoplastic flow in centered annuli, pipes, and slots, Ind. Eng. Chem. Res. **30**, 517 (1991).
[23] C. Huh and L. E. Scriven, Shapes of axisymmetric fluid interface of unbound extent, J. Colloid Interface Sci. **30**, 323 (1969).
[24] S. D. R. Wilson, The drag-out problem in film coating theory, J. Eng. Math. **16**, 209 (1982).
[25] S. D. R. Wilson, Coating flow on to rods and wires, AIChE J. **34**, 1732 (1988).
[26] D. White and J. Tallmadge, Static menisci on the outside of cylinders, J. Fluid Mech. **23**, 325 (1965).
[27] B. Geraud, L. Bocquet, and C. Barentin, Confined flows of a polymer microgel, Eur. Phys. J. E **36**, 30 (2013).
[28] L. Jørgensen, M. Le Merrer, H. Delanoë-Ayari, and C. Barentin, Yield stress and elasticity influence on surface tension measurements, Soft Matter **11**, 5111 (2015).
[29] J. Goyon, A. Colin, G. Ovarlez, A. Ajdari, and L. Bocquet, Spatial cooperativity in soft glassy flows, Nature (London) **454**, 84 (2008).
[30] R. Benzi, T. Divoux, C. Barentin, S. Manneville, M. Sbragaglia, and F. Toschi, Unified Theoretical and Experimental View on Transient Shear Banding, Phys. Rev. Lett. **123**, 248001 (2019).
[31] A. de Ryck and D. Quéré, Fluid coating from a polymer solution, Langmuir **14**, 1911 (1998).
[32] H. De Cagny, M. Fazilati, M. Habibi, M. M. Denn, and D. Bonn, The yield normal stress, J. Rheol. **63**, 285 (2019).
[33] P. Saramito, *Complex Fluids: Modeling and Algorithms* (Springer, Cham, 2016), p. 276.
[34] R. J. Gordon and W. R. Schowalter, Anisotropic fluid theory: A different approach to the dumbell theory of dilute polymer solutions, Trans. Soc. Rheol. **16**, 79 (1972).
[35] R. G. Larson, *Constitutive Equations for Polymer Melts and Solutions* (Butterworth, Stoneham, 1988), p. 132.
[36] G. M. Homsy, Viscous fingering in porous media, Ann. Rev. Fluid Mech. **19**, 271 (1987).
[37] P. Coussot, Saffman-Taylor instability in yield-stress fluids, J. Fluid Mech. **380**, 363 (1999).
[38] A. Lindner, P. Coussot, and D. Bonn, Viscous Fingering in a Yield Stress Fluid, Phys. Rev. Lett. **85**, 314 (2000).
[39] N. Maleki-Jirsaraei, B. Ghane-Motlagh, S. Baradaran, E. Shekarian, and S. Rouhani, Fractal flow of inhomogeneous fluids over smooth inclined surfaces and determination of their fractal dimensions and universality classes, J. Phys.: Condens. Matter **17**, S1209 (2005).
[40] O. A. Fadoul and P. Coussot, Saffman-Taylor instability in yield stress fluids: Theory-experiment comparison, Fluids **4**, 53 (2019).
[41] T. Divoux, A. Shukla, B. Marsit, Y. Kaloga, and I. Bischofberger, Criterion for Fingering Instabilities in Colloidal Gels, Phys. Rev. Lett. **124**, 248006 (2020).